

RESEARCH ARTICLE

10.1002/2014JD021757

Special Section:

East Asian Study of
Tropospheric Aerosols and
Impact on Cloud and
Precipitation

Key Points:

- Aerosol optical and radiative features are studied in Beijing during heavy haze
- The median radius of fine-mode particles increases as AOD increases
- Strong heating rate might exert profound impact on the atmospheric stability

Correspondence to:

J. Huang,
hjp@lzu.edu.cn

Citation:

Bi, J., J. Huang, Z. Hu, B. N. Holben, and Z. Guo (2014), Investigating the aerosol optical and radiative characteristics of heavy haze episodes in Beijing during January of 2013, *J. Geophys. Res. Atmos.*, 119, 9884–9900, doi:10.1002/2014JD021757.

Received 13 MAR 2014

Accepted 27 JUL 2014

Accepted article online 31 JUL 2014

Published online 25 AUG 2014

Investigating the aerosol optical and radiative characteristics of heavy haze episodes in Beijing during January of 2013

Jianrong Bi¹, Jianping Huang¹, Zhiyuan Hu¹, B. N. Holben², and Zhiqiang Guo³¹Key Laboratory for Semi-Arid Climate Change of the Ministry of Education and College of Atmospheric Sciences, Lanzhou University, Lanzhou, China, ²Biospheric Sciences Branch, NASA, GSFC, Greenbelt, Maryland, USA, ³Baoding City Bureau of Meteorology, Baoding, China

Abstract Several heavy atmospheric haze pollution episodes occurred over eastern and northern China during January of 2013. The pollution covered more than 100 km² and caused serious impacts on environmental quality, human health, and transportation. In this study, we characterize aerosol microphysical, optical, and radiative characteristics using a combination of ground-based Sun/sky radiometer retrievals and a radiative transfer model. Our results show that during about half of the total number of days, daily PM_{2.5} and PM₁₀ concentrations are larger than 100 μg/m³, with maxima of 462 and 433 μg/m³, respectively, during the haze events. Fine-mode (PM_{2.5}) particles dominated the aerosol size during the episodes. The volume size distribution and median radius of fine-mode particles generally increase as aerosol optical depth at 440 nm (AOD₄₄₀) increases. The median effective radius of fine-mode particles increases from 0.15 μm at low AOD value (AOD₄₄₀ ~ 0.3) to a radius of 0.25–0.30 μm at high AOD value (AOD₄₄₀ ≥ 1.0). The daily mean single-scattering albedo (SSA), imaginary part of refractive index (RI), and asymmetry factor display pronounced spectral behaviors. The overall mean SSA₄₄₀ and SSA₆₇₅ are 0.892 and 0.905, respectively. The corresponding RI₄₄₀ and RI₆₇₅ are 0.016 and 0.011, respectively. This indicates that a significant amount of absorption occurred under the haze event in Beijing during January 2013. Approximately half of the incident solar radiation energy went into heating the atmosphere as a result of strong aerosol loading and absorption. The daily averaged heating rate in the haze particle layer (0–3.2 km) varies from 0.12 to 0.81 K/day in Beijing, which might exert profound impact on the atmospheric thermodynamic and dynamical structures and cloud development, which should be further studied.

1. Introduction

As one of the major developing countries in the world, China has undergone a rapid development of its economy and industry as a result of population expansion and the emergence of many metropolitan cities since 1990. The China Statistical Bureau proclaimed that the gross domestic product (GDP) in 2012 achieved 51.6282 trillion RMB yuan, which are approximately 28 times than that of 1990 (~1.872 trillion RMB yuan). The annual growth rate of GDP in China remained steady at about 8% in the last two decades [*China Statistical Yearbook*, 2013]. The total population of China was about 1.143 billion in 1990 and increased to around 1.354 billion in 2012, which increased by nearly 211 million people. This significant growth and dramatic expansion have led to huge increases in energy consumption, emissions of air pollutants, aerosol particles, and the number of poor air quality days in mega cities along with their adjacent areas [*He et al.*, 2002; *Chan and Yao*, 2008]. Therefore, compound air pollution has become one of the primary environmental issues in China. International and domestic media often report that a thick layer of smog hanging over China's capital actually appears to be getting worse, and the increasingly hazardous amounts of air pollutants are responsible for disrupting public life.

The highly developed and densely populated metropolitan areas of Beijing, Shanghai, and Guangzhou have put forward many challenges to the Chinese environment. In particular, the emergence of a great amount of urban agglomerations (e.g., Beijing-Tianjin-Hebei, Yangtze River Delta, and Pearl River Delta economic circles) aggravates and enlarges atmospheric pollution. These massive air pollutants and fine particulate matter (also known as aerosol particles) can be breathed into the lungs which can cause serious respiratory and cardiovascular disease [*Brook et al.*, 2010]. High concentrations of atmospheric aerosols also severely deteriorate air quality and degrade visibility [*Waston*, 2002; *Molina and Molina*, 2004]. In terms of

climate impact, aerosol particles can modulate the radiation energy budget of the Earth-atmosphere system directly through scattering and absorbing solar/terrestrial radiation [Charlson *et al.*, 1992; Huang *et al.*, 2008], which in turn affects the atmospheric heating rate and stability [Huang *et al.*, 2006a; Li *et al.*, 2007, 2010]. In addition, as cloud condensation nuclei, aerosols can alter cloud droplet size, number concentration, and cloud residence time, and eventually lead to a profound influence on global precipitation and the hydrologic cycle [Ackerman *et al.*, 2000; Ramanathan *et al.*, 2001; Kaufman *et al.*, 2005; Huang *et al.*, 2006b, 2006c]. The *Intergovernmental Panel on Climate Change* [2013] pointed out that climatic impacts of aerosols still exhibit substantial uncertainties despite extensive studies that have been carried out in the last decades. This is mainly attributed to difficulties in measurement of global aerosol properties and lack of observations of some relevant parameters in addition to high spatial and temporal variability of the aerosols themselves. Hence, a full understanding of aerosol optical characteristics and their radiative effects is vital to reliably predict the future regional and global climate change.

Beijing is the capital of China and is located on the northwest margin of the Great North China Plain, surrounded by the Yanshan Mountain range, Tianjin, and the Hebei Province. The city is located in the warm temperate zone continental monsoon climate and has four distinct seasons. The total area of Beijing covers 16,410.5 km², including 16 municipal districts and two counties, with a residential population of 20.7 million. In 2012, the total amount of motor vehicles had exceeded 4.5 million, and energy consumption was equivalent to 71.8 million tons of standard coal [Beijing Statistical Yearbook, 2013]. The winter heating period in Beijing regularly begins in mid-November and ends in the following March, and it is the major source for SO₂ in winter season [He *et al.*, 2001; Hao *et al.*, 2005].

In recent years, air pollution in Beijing is typically attributed to coal burning, vehicle emissions, and long-range transport of dust, combined with stable meteorological conditions [Sun *et al.*, 2006]. To date, there have been numerous studies and investigations on aerosol characteristics as well as aerosol environmental and climatic effects in Beijing along with adjacent areas. He *et al.* [2001] and Zheng *et al.* [2005] examined the mass concentrations and chemical compositions of fine particulate matter (PM_{2.5}) in Beijing from 1999 to 2000. They found that the annual average concentrations of PM_{2.5} varied from 101 to 127 μg/m³ at different sites, with little discrepancies among the sites. In addition, carbonaceous, sulfate, nitrate, and ammonium aerosols were the major components of these fine particulate matters. Dan *et al.* [2004] characterized the carbonaceous species (organic and elemental carbon) and their sources in PM_{2.5} at urban and rural areas of Beijing and indicated that concentrations of carbonaceous species contributed 37.2 ± 12.7% of PM_{2.5} and organic carbons would constitute up to 42% of PM_{2.5} in winter. Zhang *et al.* [2013] analyzed the chemical characterization and source apportionment of PM_{2.5} in Beijing from 2009 to 2010. They concluded that the precursor gases (e.g., SO₂ and NO_x) were emitted much more in winter, and the inorganic and organic aerosols seemed to favorably form during the cold and dry winter. Sun *et al.* [2013] explored the aerosol composition, sources, and processes during the wintertime in Beijing using an Aerodyne Aerosol Chemical Speciation Monitor. They indicated that submicron aerosols showed enhanced organics and chloride during the winter, which on average accounted for 52% and 5% of the total nonrefractory submicron aerosol (NR-PM1) mass, respectively. Bergin *et al.* [2001] inspected the aerosol radiative properties and chemical compositions in Beijing during June 1999. Eck *et al.* [2005] and Xia *et al.* [2006] studied the columnar aerosol optical properties in Beijing and implied that the urban aerosols have moderate absorption as compared to the dust source regions in eastern Asia. Li *et al.* [2007] investigated the optical features and radiative effects of aerosols at Xianghe (about 70 km east of Beijing) from September 2004 to September 2005. They found that the yearly mean of aerosol optical depth at 500 nm was equal to 0.82 with a maximum greater than 4 primarily due to anthropogenic emissions. Wang *et al.* [2009b] surveyed the direct aerosol radiative forcing under clear, hazy, foggy, and dusty weather conditions over Beijing. They concluded that the daily average global solar irradiances were decreased by 30 to 40 W/m² and generated a positive heating effect on the atmosphere under haze events comparing with clear sky conditions. Li *et al.* [2013a] studied aerosol physical and chemical properties under two winter heavy haze events in Beijing using a Cimel Sun photometer. However, the knowledge of aerosol physical and chemical properties and its radiative impact under heavy haze conditions is still insufficient. Therefore, a comprehensive knowledge of aerosol optical and microphysical properties and its radiative effect on different regional scales is essential for forming a complete picture of global climate change.

A heavy atmospheric haze pollution episode occurred over eastern and northern China during 11–19 January 2013. The mass concentrations of fine particulate matter with aerodynamic diameter $<2.5 \mu\text{m}$ ($\text{PM}_{2.5}$) in many cities have exceeded the range of measurement. For instance, the maximum hourly concentration values of $\text{PM}_{2.5}$ in Beijing were more than $600 \mu\text{g}/\text{m}^3$ and even approached $1000 \mu\text{g}/\text{m}^3$, which is 10 times larger than the Chinese secondary standard value ($\sim 75 \mu\text{g}/\text{m}^3$). The Chinese Environmental Protection Bureau (CEPB) reported that air quality in 33 cities was seriously polluted during the period as observed by 74 environmental monitoring stations throughout China. For example, a severe haze episode covered a region of more than 100km^2 and significantly affected human health and transportation. This event also drew the extensive attention of scientists and governments around the world. In fact, the China Meteorological Administration claimed that there were only five clear-sky days in January 2013 with five serious haze pollution episodes occurring in Beijing during that time. Note that the events lasted anywhere from 3 to 7 days. In this article, we analyze the mass concentrations of particulate matter from in situ measurements, aerosol microphysical, optical, and radiative characteristics using a combination of ground-based Sun/sky radiometer and radiative transfer model during the heavy haze episodes of 2013.

2. Site Description and Instrumentation

2.1. Site Description

There are three sites located in the north urban area of Beijing, and all are equipped with a Cimel Electronique Sun/sky radiometer (Model CE-318). They include the following: the Chinese Academy of Meteorological Sciences (CAMS, 39.933°N , 116.317°E , 105 m above mean sea level (msl)), Institute of Atmospheric Physics (IAP, 39.977°N , 116.381°E , 92 m above msl), and Institute of Remote Sensing and Digital Earth, Chinese Academy of Sciences (RADI, 40.005°N , 116.379°E , 59 m above msl). The instruments are installed on the rooftops of the CAMS, IAP, and RADI sites. The CAMS site belongs to China Aerosol Remote Sensing Network [Che *et al.*, 2009], which was established by the China Meteorological Administration for studying dust aerosol optical properties over different areas in China since 2002. The IAP site is one of AEROSOL ROBOTIC NETWORK (AERONET) and PHOTOMETRIE POUR LE TRAITEMENT OPERATIONNEL DE NORMALISATION SATELLITAIRE sites, which are two well-known ground-based aerosol-monitoring networks using Cimel Sun photometer. The IAP site has been operational since March 2002 and surveyed aerosol optical properties over the north urban area of Beijing [Xia *et al.*, 2006]. RADI is an AERONET facility that is operated by the Institute of Remote Sensing and Digital Earth of the Chinese Academy of Sciences [Li *et al.*, 2013a]. The instrument calibrations of direct solar measurement are carried out by the Langley plot technique that compares AERONET retrievals with the master instruments deployed at Waliguan Observatory (36.283°N , 100.896°E , 3816 m above msl), IZANA observatory (28.309°N , 16.499°E , 2391 m above msl), and Litang site (29.976°N , 100.262°E , 3913 m above msl) once per year or every 6 months, respectively. The sky radiances of Sun/sky radiometer are calibrated by a 2 m integrating sphere at the laboratories mentioned above, with an absolute accuracy of 3%–5% [Li *et al.*, 2008].

2.2. Particulate Matter Measurements

In this paper, we defined fine particulate matter with aerodynamic diameter less than $2.5 \mu\text{m}$ as $\text{PM}_{2.5}$ and inhalable particulate matter with diameter less than $10 \mu\text{m}$ as PM_{10} . The continuous in situ $\text{PM}_{2.5}$ and PM_{10} monitors are based on inertial mass weighing principle (Rupprecht and Patashnick Tapered Element Oscillating Microbalance (TEOM)) and electron absorption (Andersen Instruments and Wedding and Associates Beta Attenuation Monitors (BAM)) [U. S. Environmental Protection Agency (EPA), 1990, 1991], which are designated as the equivalent methods for measuring $\text{PM}_{2.5}$ and PM_{10} . The daily mean values of $\text{PM}_{2.5}$ and/or PM_{10} are simultaneously measured at the U.S. Embassy and Chinese Environmental Protection Bureau (CEPB) in $\mu\text{g}/\text{m}^3$ (www.chinaairdaily.com). The CEPB relies on TEOM method measured at several urban sites in Beijing, and the U.S. Embassy uses the BAM method and is located about 10 km southeast of RADI site.

2.3. Sun/Sky Radiometer Measurements

The detailed information of the instrument, operation, and calibration is discussed in Holben *et al.* [1998]. The Cimel Sun/sky radiometers take measurements of direct solar irradiance at 340, 380, 440, 500, 675, 870, 940, and 1020 nm (nominal wavelengths), with a 1.2° full field of view every 15 min. The Sun photometer performs three measurements of direct Sun irradiance for each band within 1 min, which is employed to calculate

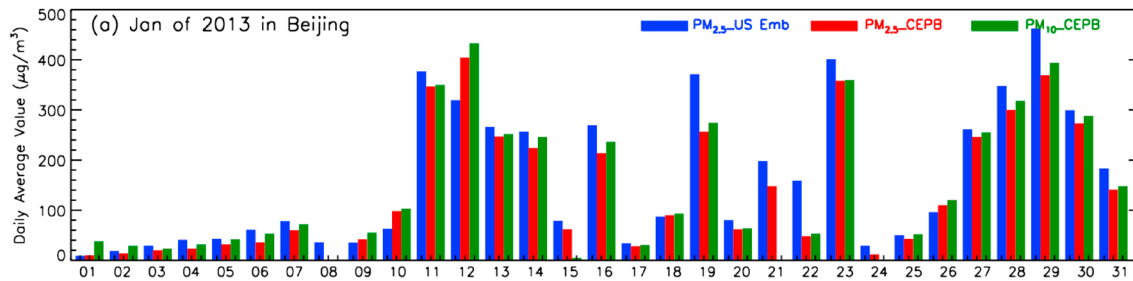


Figure 1. Daily mean mass concentration of $PM_{2.5}$ sampled at the U.S. Embassy (blue), Chinese Environmental Protection Bureau (CEPB, red), and PM_{10} at CEPB (green) during January of 2013 in Beijing.

columnar total optical depth as well as detect and eliminate cloud contamination [Smirnov *et al.*, 2000]. The measurement of 940 nm band is capable of computing total precipitable water vapor content (WVC) in centimeters. Bi *et al.* [2013] documented that the precipitable WVC acquired from the Cimel Sun photometer is consistent with radiosonde measurements within the expected observational uncertainty. The half bandwidths of 340 and 380 nm wavelengths are 2 nm and 4 nm, and about 10 nm for other channels. In addition, the Sun photometer makes the angular sky radiance scan in an almucantar and solar principal plane geometry for intensity and polarization measurements [Li *et al.*, 2013a], which can be used to simultaneously retrieve aerosol size distribution, complex refractive index, and single-scattering albedo. Eck *et al.* [1999] estimated that the total uncertainty in AOD for a newly calibrated field instrument is about 0.010–0.021 (which is spectrally dependent with the higher errors in UV). The retrieval errors of single-scattering albedo (SSA) are expected to be 0.03–0.05 depending on aerosol types and loading [Dubovik *et al.*, 2000]. It is worth noting that this uncertainty of SSA is based on $AOD_{440} \geq 0.4$ and for solar zenith angle $> 50^\circ$ (Level 2.0 product), and the uncertainty will become much larger when $AOD_{440} < 0.4$. The data sets used in this study come from the Level 2.0 at IAP and Level 1.5 at CAMS and RAD (when the Level 2.0 data were unavailable) quality-assured data (<http://aeronet.gsfc.nasa.gov>). The data are prefield and postfield calibrated and automatically cloud screened [Smirnov *et al.*, 2000]. Note that a spheroid particle shape assumption with a fixed aspect ratio distribution is used to retrieve aerosol single-scattering properties during the serious haze periods [Dubovik *et al.*, 2006].

3. Results and Analysis

3.1. Aerosol Optical Characteristics

Figure 1 shows the daily mean mass concentration of $PM_{2.5}$ sampled at the U.S. Embassy and CEPB, and PM_{10} at CEPB during January of 2013 in Beijing. The daily average concentrations of $PM_{2.5}$ at the U.S. Embassy are mostly higher than that at CEPB, which is attributed to different instrument types and different sampling locations. In spite of this, the tendencies of daily averaged $PM_{2.5}$ at the U.S. Embassy are consistent with CEPB. Additionally, the daily mean variations of PM_{10} exhibit the same features as $PM_{2.5}$. It is clear that both the $PM_{2.5}$ and PM_{10} concentrations present striking day-to-day variations during the whole period. About 50% of the total number days of $PM_{2.5}$ and PM_{10} are larger than $100 \mu\text{g}/\text{m}^3$, with maxima of 462 and $433 \mu\text{g}/\text{m}^3$, respectively, which are 18 times and 8 times higher than World Health Organization Air Quality Guidelines of $25 \mu\text{g}/\text{m}^3$ for $PM_{2.5}$ and $50 \mu\text{g}/\text{m}^3$ for PM_{10} (24 h average), respectively [World Health Organization, 2005]. Several episodes with high $PM_{2.5}$ and PM_{10} concentrations are evident and include: 6–8 January 2013 (with $PM_{2.5}$ of 36 – $78 \mu\text{g}/\text{m}^3$), 9–15 January (with $PM_{2.5}$ of 42 – $404 \mu\text{g}/\text{m}^3$), 16–19 January (with $PM_{2.5}$ of 34 – $371 \mu\text{g}/\text{m}^3$), 20–23 January (with $PM_{2.5}$ of 62 – $358 \mu\text{g}/\text{m}^3$), and 25–31 January (with $PM_{2.5}$ of 43 – $462 \mu\text{g}/\text{m}^3$). These episodes coincide well with the aforementioned heavy haze events during January of 2013. The ratios of $PM_{2.5}$ to PM_{10} always remain at above 0.70 under haze days, almost of which are larger than 0.90 for the heavy haze cases. The ratio values on 1 and 2 January 2013 are 0.26 and 0.48, respectively, which are the only two clear sky days having ratios less than 0.70. Our results indicate that fine particle pollution during January of 2013 is unprecedentedly severe in Beijing urban area. The overall daily mean $PM_{2.5}$ and PM_{10} at CEPB site is about 143.9 and $157.8 \mu\text{g}/\text{m}^3$, respectively, which is comparable to the annual average concentration in previous research results (e.g., $PM_{2.5}$ ranging from 101 to $127 \mu\text{g}/\text{m}^3$ at different sampling sites in Beijing).

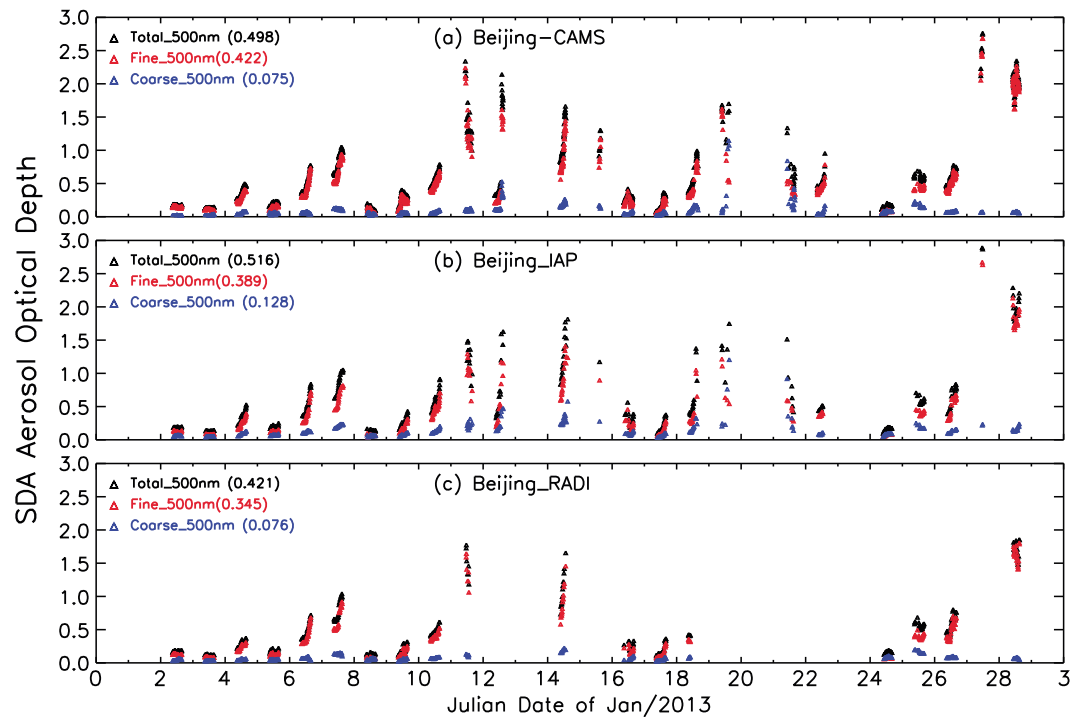


Figure 2. Time series of total (black), SDA fine-mode (red), and coarse-mode (blue) AOD at 500 nm obtained from Sun photometer measurements at (top) CAMS, (middle) IAP, and (bottom) RADI sites during January of 2013. Overall average values are in parentheses.

Nevertheless, as compared with previous haze episodes, this event not only had a longer duration of elevated $PM_{2.5}$ concentration but also had a larger spatial coverage. This undoubtedly led to stronger deleterious effects on air quality and climate.

Aerosol optical depth (AOD) and Ångström exponent are two robust parameters for characterizing aerosol optical properties and determining the magnitude of aerosol direct radiative forcing. Ångström exponent α is the slope of the logarithm of AOD (τ_a) versus the logarithm of wavelength ($\ln \lambda$). We apply a log-linear fitting based on four wavelengths in the range 400–870 nm to compute the value of α , i.e., $\lambda = 440, 500, 675,$ and 870 nm (the IAP site is polarized Cimel Sun photometer and does not have the 500 nm channel). The α is commonly used to describe the wavelength dependence of τ_a and to provide some basic information on aerosol size distribution [Eck *et al.*, 1999]. For instance, small α around zero represents large dust particles whereas large α around 2.0 corresponds to small particles [Dubovik *et al.*, 2002]. O'Neill *et al.* [2001, 2003] developed a spectral deconvolution algorithm (SDA) to extract the components of fine and coarse-mode optical depths from the spectral total extinction aerosol optical depth data. The SDA procedure is primarily based on two fundamental assumptions. The first is that the aerosol particle size distribution (PSD) is effectively bimodal. The second hypothesis is that the coarse-mode Ångström exponent and its spectral variation are both approximately neutral. Ångström exponent and its second derivative (as parameterized by $\alpha' = d\alpha/d \ln \lambda$) are the measurement inputs to the SDA. These continuous function derivatives (usually computed at a reference wavelength of 500 nm) are derived from a second-order polynomial fit of $\ln \tau_a$ versus $\ln \lambda$ [Eck *et al.*, 1999]. The spectral AOD utilized as input to SDA were limited to six Cimel bands at 380, 440, 500, 675, 870, and 1020 nm wavelengths.

Figure 2 depicts the time series of total, SDA fine-mode, and coarse-mode AOD_{500} generated from Sun photometer measurements at the CAMS, IAP, and RADI sites during January of 2013. Note that the Level 2.0 product of cloud screened data at IAP site is employed in SDA procedure to infer AOD spectra, while the Level 1.5 products are applied at CAMS and RADI sites. AOD at the three sites display the same pattern of diurnal variations. For example, the overall mean values of total, SDA fine and coarse-mode AOD_{500} at CAMS site are about 0.50 (0.08–2.76), 0.42 (0.05–2.69), and 0.08 (0.01–1.15), respectively. It is obvious that the

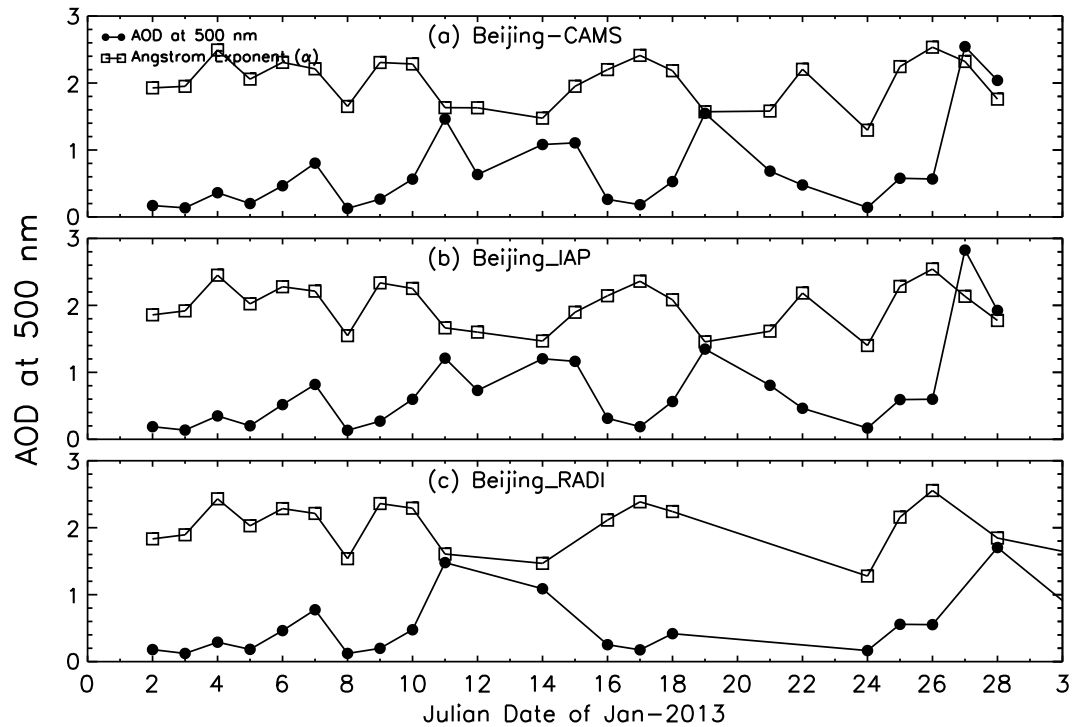


Figure 3. Daily mean of aerosol optical depth (AOD) at 500 nm and Ångström exponent (440–870 nm) at (a) CAMS, (b) IAP, and (c) RADl sites during January of 2013.

coarse-mode AOD_{500} is generally small and nearly constant, while the fine-mode AOD_{500} of haze particles exhibits dramatic diurnal variations. There are only some cases of the coarse-mode AOD_{500} to be comparable with the fine-mode AOD_{500} (e.g., 19 and 21 January), possibly owing to dust transported from Inner Mongolia or from residual cloud contamination. The overall average values of SDA fine-mode fraction (FMF, denoted as fine-mode AOD_{500} divided by total AOD_{500}) are 0.804 (0.326–0.977), 0.687 (0.311–0.933), and 0.748 (0.421–0.973) for the three sites, respectively. The daily mean FMF values at the three sites during heavy haze event (28 January) are 0.965, 0.933, and 0.973, respectively, which are somewhat larger than the mean value of 0.93 at the RADl site under two heavy haze episodes in 2011 and 2012 [Li *et al.*, 2013a]. The time series of total and fine-mode AOD_{500} show consistent variations with the concentrations of particulate matter (e.g., $PM_{2.5}$ or PM_{10}).

Figure 3 shows the daily mean of AOD_{500} and Ångström exponent (440–870 nm) at CAMS, IAP, and RADl sites, respectively, during January of 2013. The daily average data are calculated from all points for each day when three or more points are available. AOD_{500} at the three sites present similar daily mean features, with notable day-to-day variations, and vary from near background levels of 0.10 to polluted haze day with values exceeding 2.80. This suggests that AOD_{500} measured at three city sites in Beijing can be representative of the urban area. The overall mean of AOD_{500} are 0.71 ± 0.63 , 0.72 ± 0.64 , and 0.51 ± 0.47 for the three sites, respectively, which are much higher than the multiyear average AOD_{500} of ~ 0.40 during January at Beijing IAP site [Eck *et al.*, 2005]. Xia *et al.* [2006] analyzed 33 months of AERONET aerosol data at Beijing_IAP site and also indicated that AOD increased from January to June and then gradually decreased. This means, comparing with multiyear averages, the optical extinctions of aerosol particles are extremely strong under the heavy haze episodes in Beijing during January of 2013. And the corresponding mean values of α are 1.21 ± 0.21 , 1.19 ± 0.21 , and 1.13 ± 0.26 , respectively, which are comparable to the multiyear average of ~ 1.25 presented by Eck *et al.* [2005]. The Ångström exponent remains consistently elevated (e.g., ranging from 0.78 to 1.52 at CAMS site) during the entire period, regardless of low AOD_{500} values (e.g., ranging from 0.13 to 2.54 at CAMS site), which is completely different from dust cases [Bi *et al.*, 2013]. Nearly all the values of Ångström exponent are larger than 0.85, which indicates that small pollution particles are the main contributors to aerosol optical depth in Beijing during the heavy haze of 2013.

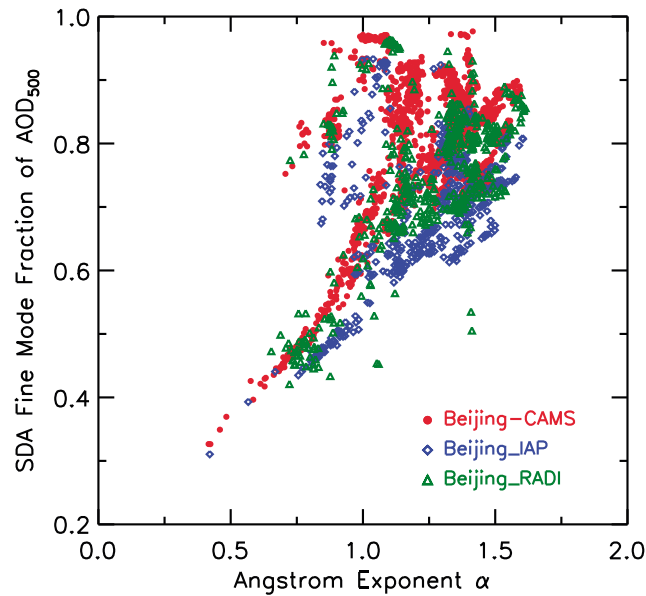


Figure 4. Spectral deconvolution algorithm (SDA) computed instantaneous fine-mode fraction of AOD₅₀₀ versus Ångström exponent (440–870 nm) at Beijing-CAMS (red circle), Beijing_IAP (blue diamond), and Beijing_RAD1 (green triangle) sites.

Figure 4 illustrates the spectral deconvolution algorithm (SDA) computed instantaneous FMF of AOD₅₀₀ versus Ångström exponent (440–870 nm) at Beijing-CAMS, Beijing_IAP, and Beijing_RAD1 sites. The values of FMF at the three sites vary from 0.30 to 1.0. It is worth noting that FMF significantly increases with Ångström exponent (440–870 nm), which is anticipated because a larger Ångström exponent is often related to smaller haze particles. Furthermore, with the increase of FMF, the Ångström exponent displays much more dispersive for a fixed FMF value (e.g., FMF = 0.8), which was primarily attributed to the different variations between fine-mode particle size and Ångström exponent when fine-mode particles augment from hygroscopic growth. *Li et al.* [2013a]

inferred the geometric hygroscopic growth factors (gHGF) of aerosol are 1.11 and 1.17 in Beijing_RAD1 site during the two heavy haze events in 2011 and 2012. And *Schuster et al.* [2009] indicated that aerosol particles would be hygroscopic and grew in the presence of water, when the gHGF is larger than 1.0. Another remarkable feature is that Ångström exponent keeps relatively low values (e.g., ranging from 0.60 to 1.0) when FMF values vary within 0.70 to 1.0 at the three sites. This suggests that accumulated mode particles also may exist in Beijing during January of 2013.

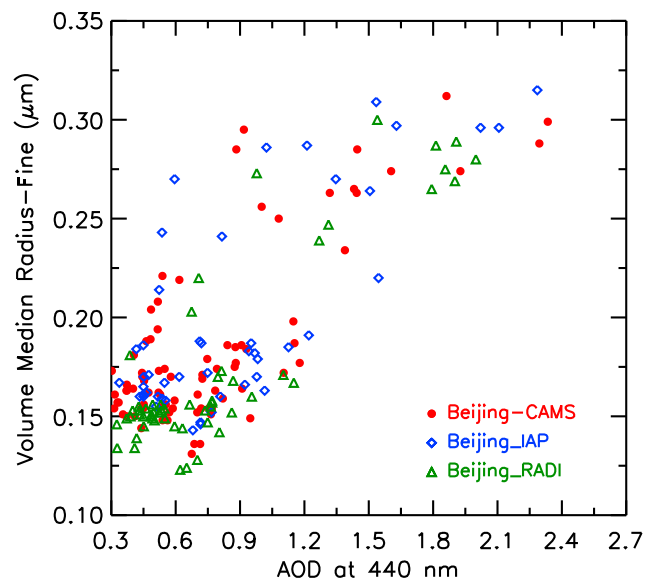
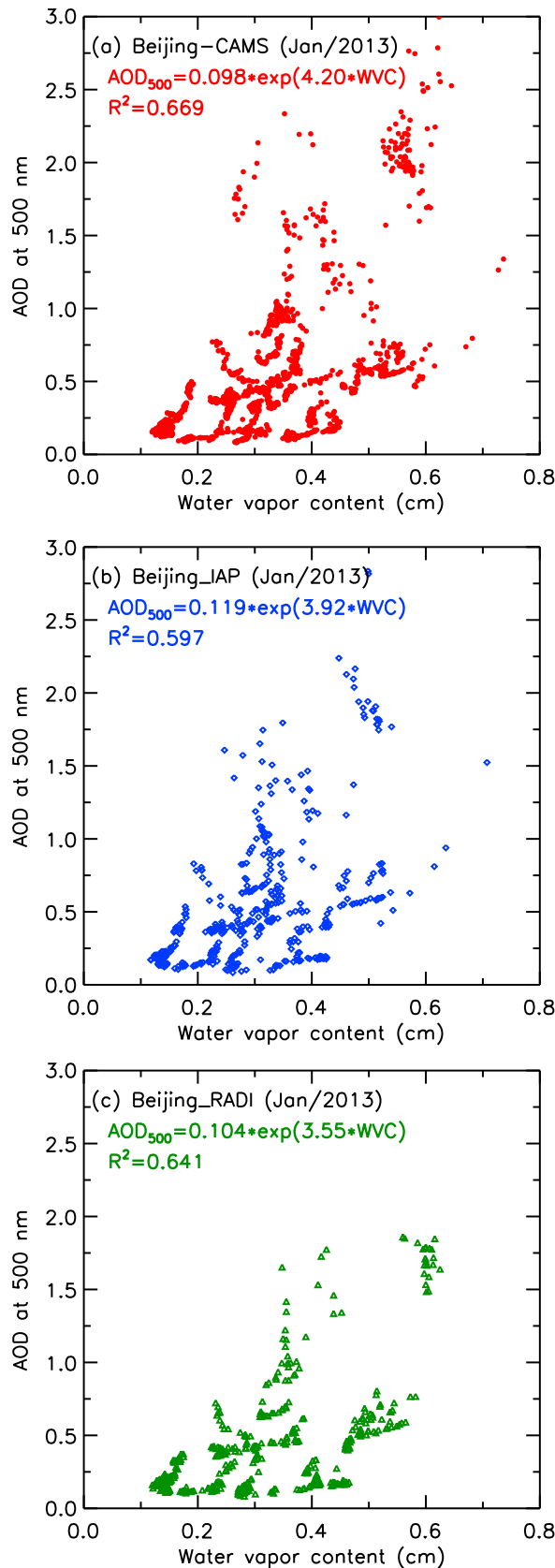


Figure 5. Fine-mode volume median effective radius versus AOD₄₄₀ at Beijing-CAMS (red circle), Beijing_IAP (blue diamond), and Beijing_RAD1 (green triangle) sites, corresponding to AOD₄₄₀ larger than 0.30. It shows a general increase in volume median effective radius with increasing AOD₄₄₀ ($R^2 = 0.77, 0.75, \text{ and } 0.87$, respectively).

Figure 5 delineates the relationship between the instantaneous fine-mode volume median effective radius and AOD₄₄₀ at the three sites during the period. In order to eliminate the influences of background aerosols, we only present those values of AOD₄₄₀ greater than or equal to 0.30. The volume median radius of fine-mode particles generally increases as AOD₄₄₀ increases. The volume median radius of fine-mode particles increases from 0.15 μm at low AOD (AOD₄₄₀ ~ 0.3) to a radius of 0.25–0.30 μm at high AOD (AOD₄₄₀ ≥ 1.0) under heavy haze episodes. And the corresponding correlation coefficients (R^2) are equal to 0.77, 0.75, and 0.87, respectively, for the three sites. The cause of larger size fine-mode particles at higher AOD is likely due to the increasing rates of coagulation as AOD (and therefore concentration) increases [*Eck et al.*, 2005]. This indicates that very large



accumulation mode particles are generated under heavy haze events in Beijing due to extremely high concentrations of fine particulate matter that can lead to coagulation through both condensation and gas-to-particle conversion processes [Reid and Hobbs, 1998; Eck et al., 2001]. This conclusion can be demonstrated by Figure 6, which displays the relationship between the instantaneous AOD_{500} and columnar water vapor content (WVC) for Beijing-CAMS, Beijing_IAP, and Beijing_RADI sites. Strong positive correlations are found for the three sites with correlation coefficients of 0.669, 0.597, and 0.641, respectively. And the corresponding exponential fit equations are $AOD_{500} = 0.098 \times \exp(4.2 \times WVC)$, $AOD_{500} = 0.119 \times \exp(3.92 \times WVC)$, and $AOD_{500} = 0.104 \times \exp(3.55 \times WVC)$, respectively. In fact, Kotchenruther et al. [1999] also implied that the small particles would undergo hygroscopic growth with the increase of relative humidity.

3.2. Spectral Behavior of Aerosol Properties

Figure 7 characterizes the time series variations of AOD at five wavelengths and Ångström exponent (440–870 nm) under the clear sky and haze days at CAMS site from Sun photometer measurements. The clear sky days are identified as $AOD_{440} < 0.30$ and $\alpha > 1.0$ (J. Bi et al., Dust aerosol characteristics and shortwave impact at a Gobi Desert of northwest China during the spring of 2012, submitted to *Journal of the Meteorological Society of Japan*, 2013), whereas the haze days are identified as $AOD_{440} > 1.0$ and $\alpha > 1.0$ [Li et al., 2013a]. The AOD values under clear sky conditions are low (with all AOD less than 0.24) and maintain slight variations, although Ångström exponent values remain relatively high (ranging from 0.87 to 1.23). For heavy haze cases, the AOD at each wavelength maintain

Figure 6. Scatterplots of the instantaneous aerosol optical depth at 500 nm (AOD_{500}) versus water vapor content (WVC) in centimeters for (a) Beijing-CAMS, (b) Beijing_IAP, and (c) Beijing_RADI sites during the whole period.

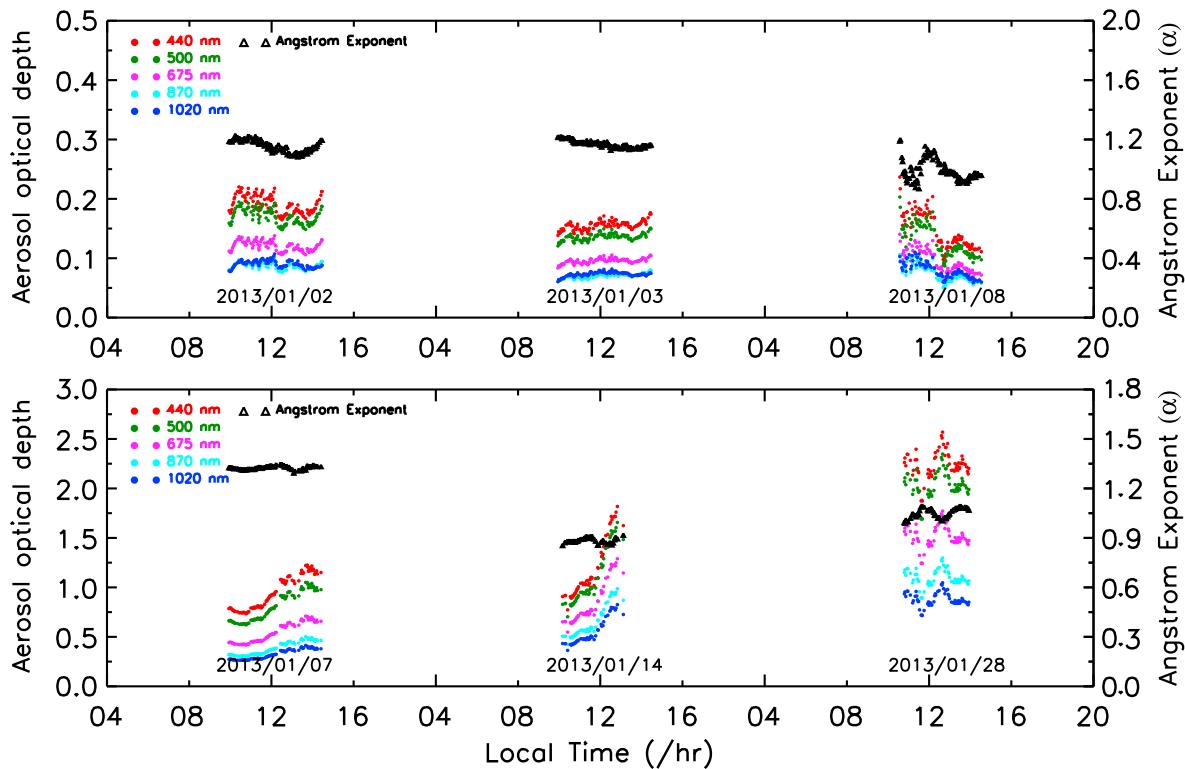


Figure 7. Time series variations of aerosol optical depth (AOD) at five wavelengths and Ångström exponent (440–870 nm) under the (top) clear sky and (bottom) clear haze days at CAMS site from Sun photometer measurements.

comparatively high values with the maximum AOD_{440} of 2.5 on 28 January 2013. The corresponding Ångström exponent varies from 0.9 to 1.35 under haze events. A notable increasing tendency observed on 7 and 14 January which corresponds to the formation of haze processes. It is very interesting that AOD at each wavelength on 7 January (daily mean $AOD_{440} \sim 0.94$) is smaller than that of 28 January (daily mean $AOD_{440} \sim 2.24$), while the corresponding Ångström exponent on 7 January (~ 1.33) is bigger than that of 28 January (~ 1.05). This reveals that either more fine-mode particles or smaller radius of fine-mode particles appear on 7 January in Beijing.

Figure 8 depicts the daily mean spectral values of (a) aerosol optical depth and (b) retrieved volume size distributions during different days. We distinguish the clear sky and haze days according to the criteria mentioned above. We find that 8 January 2013 is the sole clear sky day while the other days have different degrees of haze. From Figure 8, we know that the slopes of $\ln \tau_a$ versus $\ln \lambda$ are equal to or greater than 1.0, although the daily mean of AOD_{440} range from 0.14 under background level to 2.24 under heavy haze event, which suggests again that small particles are dominant in Beijing during January of 2013. Dubovik *et al.* [2002] confirmed that the retrieval errors of volume size distribution do not exceed 10% for the intermediate particle size range ($0.1 \leq r \leq 7 \mu\text{m}$) and may greatly increase at the edges of the range ($r > 0.1 \mu\text{m}$ or $r < 10 \mu\text{m}$). Figure 8b exhibits an obvious bimodal pattern of size distribution for all days. The fine-mode particles are predominant and dramatically change during the haze days, while corresponding coarse-mode particles remain relatively constant. The volume concentration ratio of fine-mode particle to coarse-mode particle (C_{vf}/C_{vc}) ranges from about 0.20 at background level day (8 January) to 2.36 at heavy haze day (28 January). The mean radius of fine-mode particles increase from $0.157 \mu\text{m}$ at low AOD_{440} (~ 0.14) to $0.287 \mu\text{m}$ at high AOD_{440} (~ 2.24), which is consistent with the results presented in Figure 5. Additionally, the volume size distributions of fine-mode particles steadily increase with the increasing of AOD, which indicates that the radius and size distribution of fine-mode particles simultaneously increase during the process of hygroscopic growth.

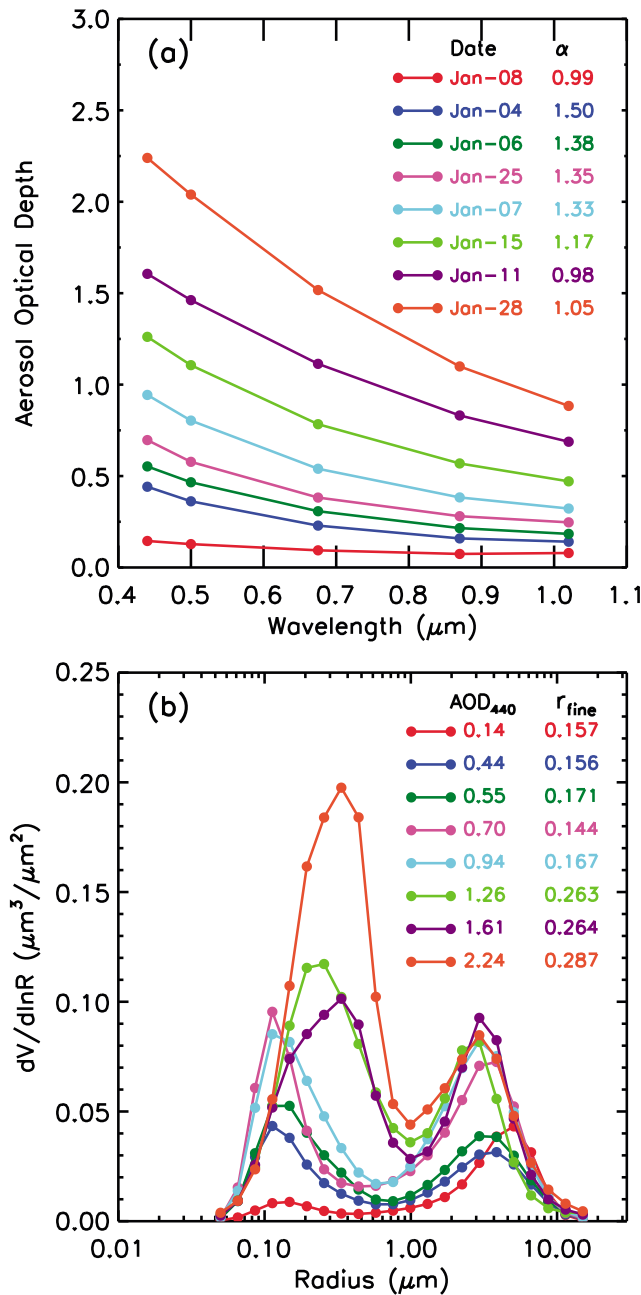


Figure 8. Daily mean spectral values of (a) aerosol optical depth and (b) retrieved aerosol volume size distributions under different days.

although haze particles can strongly scatter the sunlight, the mean absorption of aerosol in Beijing is very strong during January 2013.

The imaginary part of complex refractive index is an important physical quantity for characterizing the absorbing property of aerosol. Figure 9b presents an opposite change tendency of RI comparing with SSA, namely, RI values generally decrease from 440 nm to 675 nm and increase from 675 nm to 1020 nm under haze days. The enhanced absorption (larger imaginary part or smaller SSA) at 440 nm indicates the presence of spectrally dependent absorbing aerosols (e.g., organic carbon or dust) [Bond and Bergstrom, 2006]. The overall mean values of RI_{440} and RI_{675} are 0.016 and 0.011, which are comparable to the averaged RI_{440} and RI_{675} are 0.013 and 0.008 under two heavy haze events in 2011 and 2012 at Beijing_RADI site [Li et al., 2013a]. Correspondingly, the AAOD significantly decreases from 440 nm to 675 nm and remains typically invariant from 675 nm to 1020 nm.

Figure 9 describes the daily mean spectral values of single-scattering albedo (SSA), imaginary part of complex refractive index (RI), asymmetry factor (ASY), and absorption aerosol optical depth (AAOD). Both the values of SSA and ASY remarkably increase with the increasing of AOD, with a changed range of SSA varying from 0.07 to 0.12 and ASY ranging from 0.09 to 0.20 (corresponding to AOD_{440} from 0.10 to 2.24). This implies that aerosol particles are strongly scattering during haze conditions, which may be attributed to more nonabsorbing particles (e.g., nitrates, sulfates, and ammonium sulfates) generated during the hygroscopic growth process. SSA value is commonly increased from 440 nm to 675 nm and decreased from 675 nm to 1020 nm during haze cases. A possible reason is partly ascribed to the influence of organic carbon that constitutes up to 42% of $\text{PM}_{2.5}$ during the winter in Beijing [Dan et al., 2004]. Sun et al. [2013] also suggested that the enhanced organics account for about 52% of the total nonrefractory submicron aerosol mass during the winter in Beijing. The overall averages of SSA_{440} and SSA_{675} are 0.892 and 0.905 under haze cases, corresponding ASY_{440} and ASY_{675} are 0.685 and 0.635. Our results are close to the multiyear average SSA_{440} of 0.90 at Beijing IAP site [Xia et al., 2006] and Mexico City ($\text{SSA}_{550} \sim 0.89$) but less than that in Maryland ($\text{SSA}_{550} \sim 0.97$) and Paris ($\text{SSA}_{550} \sim 0.93\text{--}0.94$) [Dubovik et al., 2002]. Our results indicate that

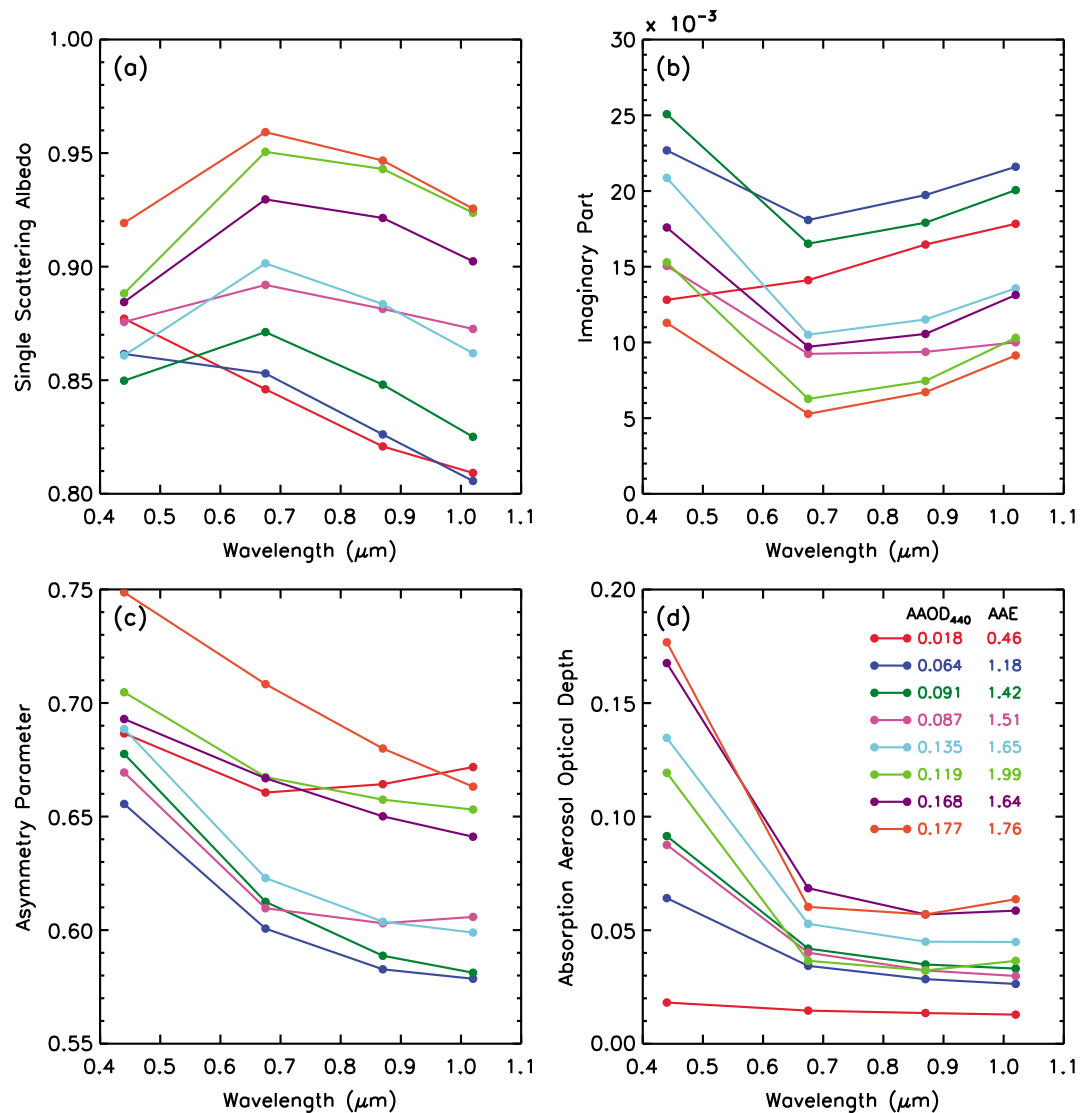
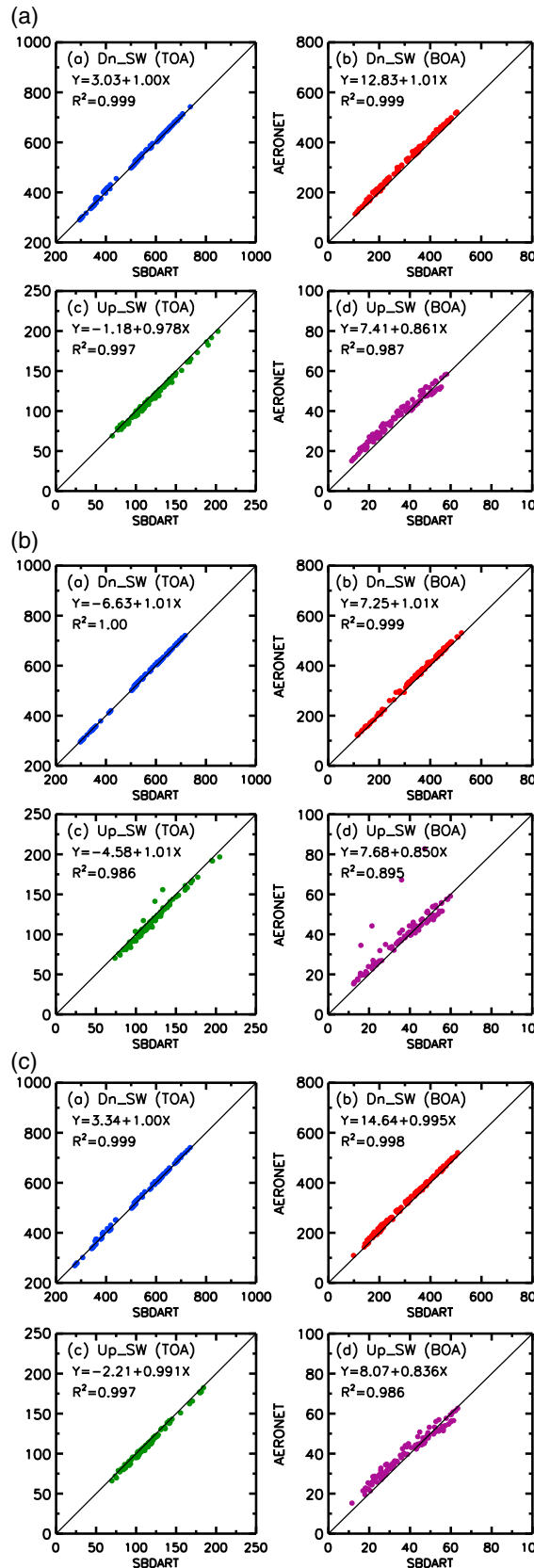


Figure 9. Daily averaged spectral values of the retrieved (a) single-scattering albedo, (b) imaginary part of complex refractive index, (c) asymmetry parameter, and (d) absorption aerosol optical depth. Note that the color codes of lines in each panel are the same as in Figure 8.

4. Aerosol Direct Radiative Effect

4.1. Radiative Transfer Model

The Santa Barbara Discrete-ordinate Atmospheric Radiative Transfer (SBDART) model is a code to calculate the solar radiations within the Earth's atmosphere and at the surface under clear and cloudy conditions [Ricchiuzzi *et al.*, 1998]. Version 2.4 of the software is used in this paper, which is based on the four stream discrete ordinate approximation and atmospheric transmission data computed by the LOWTRAN-7, fit with a three-term exponential sum. *Halothore et al.* [2005] and *Bi et al.* [2013] verified that the broadband spectrum irradiance modeled by SBDART coincides well with ground-based observations (less than 3%). The key input parameters to run the model include: AOD, SSA, and ASY at 440, 675, 870, and 1020 nm along with Ångström exponent, columnar water vapor content, total ozone amount, and spectral surface albedo. The aerosol optical properties at four AERONET wavelengths are applied to interpolate and extrapolate the spectral bands of SBDART. The columnar water vapor content is retrieved from the Cimel Sun photometer. The daily ozone amount is derived from the Total Ozone Mapping Spectrometer (TOMS, <http://toms.gsfc.nasa.gov>), which varied from 348 to 361 DU in our study. The spectral surface albedo is inferred from the 500 m resolution Moderate Resolution



Imaging Spectroradiometer (MODIS) bidirectional reflectance distribution function/Albedo products [Moody *et al.*, 2005]. Finally, we can utilize the SBDART model to estimate the surface radiation fluxes from 0.20 to 4.0 μm spectral bands.

4.2. Comparison Between SBDART Simulations and AERONET Products

Figure 10 presents the comparisons between SBDART-simulated and AERONET-retrieved products of downward and upward shortwave radiations at the top of atmosphere (TOA) and the surface (BOA). In the AERONET algorithm, the modeling of atmospheric radiance is performed by publicly available discrete ordinates radiative transfer codes [Dubovik and King, 2000]. Our results show excellent agreements for downward shortwave radiation fluxes at TOA and the surface, with the correlation coefficients greater than 0.998 for all cases. The corresponding mean differences and standard deviations range from 2.03 to 11.7 W m^{-2} , and from 3.28 to 6.05 W m^{-2} , respectively. This is taken for granted because the main input quantities of SBDART and AERONET models are the same. If we could obtain the direct and diffuse radiation fluxes from ground-based observations, we can inspect the detailed accuracy of spectral AOD, SSA, and ASY, along with total precipitable water. However, many investigators have performed excellent shortwave radiative closure experiment using the accurate input parameters from AERONET and high-precision surface radiation fluxes [Wang *et al.*, 2009a; Bi *et al.*, 2013], which confirmed that the spectral aerosol optical properties from AERONET are reasonable and reliable. Moreover, the SBDART modeled upward radiation quantity at TOA is slightly greater than that from AERONET which is in contrast to what occurs at the surface. This is mainly ascribed to the different input spectral surface reflectance for the radiative transfer model. In our study, the spectral surface reflectance is derived from the 500 m resolution MODIS

Figure 10. Comparisons between the SBDART simulated and AERONET inversion products of downward shortwave radiations at (a) TOA and (b) surface (BOA), upward shortwave radiations at (c) TOA and (d) surface in CAMS, IAP, and RADI sites.

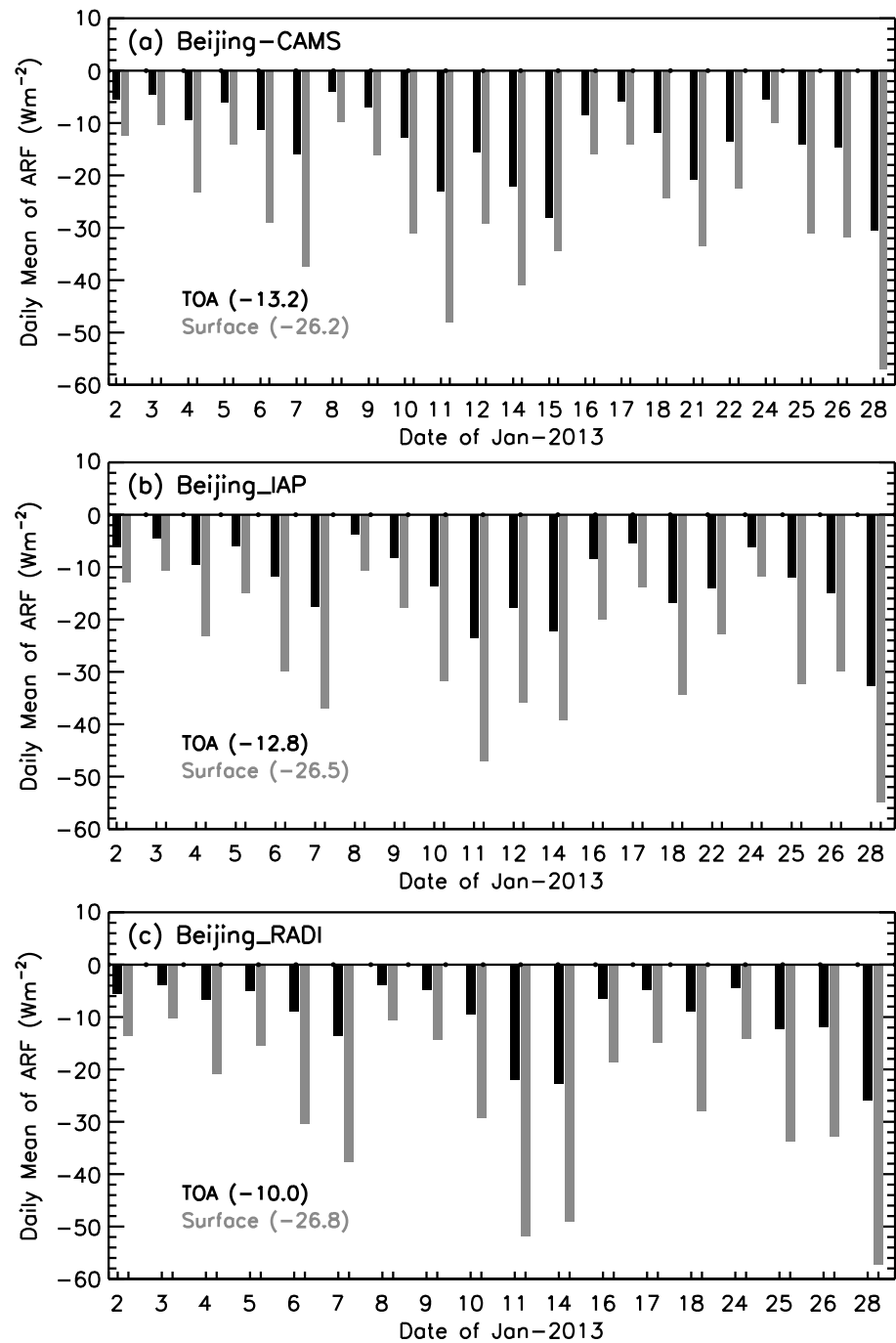


Figure 11. Daily average values of aerosol direct radiative forcing at the surface (grey bars) and TOA (black bars) in (a) CAMS, (b) IAP, and (c) RAD1 sites.

bidirectional reflectance distribution function/Albedo products, and the corresponding value is accounted for using a priori climatological data in AERONET [Dubovik and King, 2000]. In general, the mean differences of downward shortwave radiation fluxes are smaller than 6% and 11% for the upward radiation fluxes.

4.3. Aerosol Direct Radiative Forcing and Heating Rate

Aerosol direct shortwave radiative forcing (ARF) is defined as the difference between the net shortwave radiation fluxes with and without aerosols under cloud-free conditions. A detailed method is discussed by recent publications [Ge et al., 2010; Bi et al., 2013]. In this study, we determine ARF from a

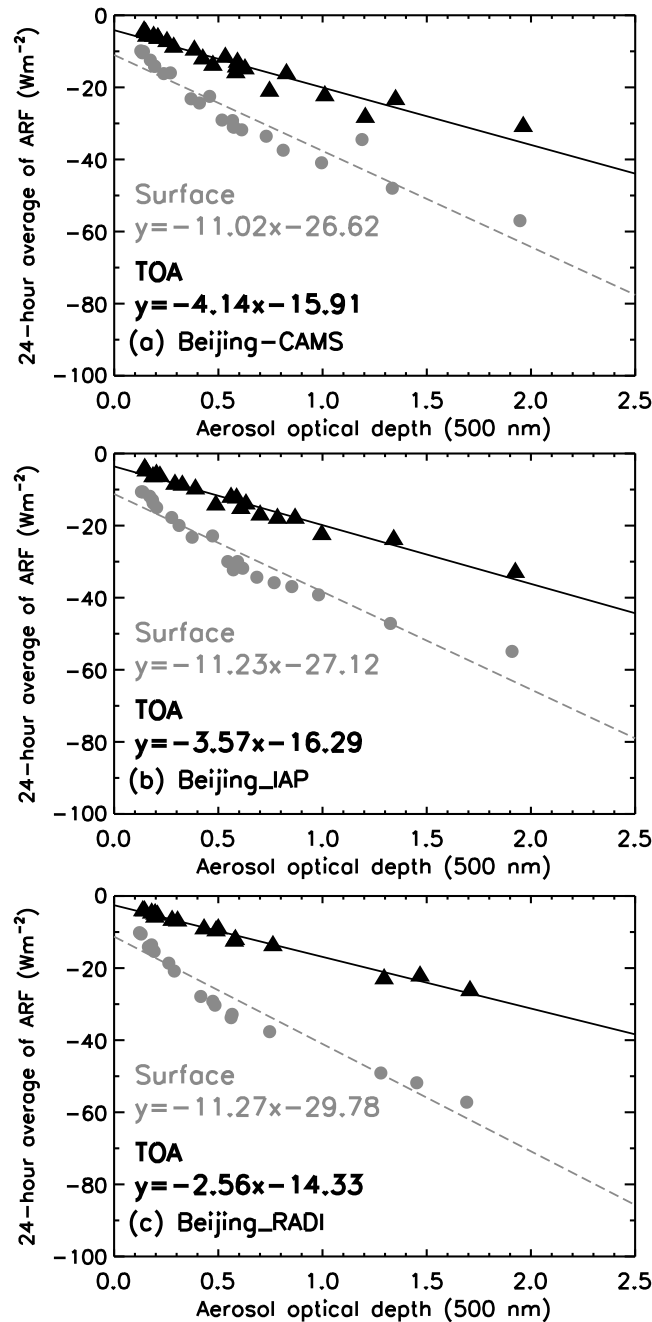


Figure 12. Correlation between daily mean aerosol direct radiative forcing and AOD₅₀₀ at the surface (grey circles) and TOA (black triangles) in (a) CAMS, (b) IAP, and (c) RADI sites.

and $-10.0 \pm 6.9 \text{ W m}^{-2}$, and hence forcing values in the atmosphere are $+13.0 \pm 6.5$, $+13.8 \pm 5.8$, and $+16.8 \pm 8.1 \text{ W m}^{-2}$ for the three sites, respectively. High ARF values at the surface are coincident with the large AOD values. Yu *et al.* [2006] evaluated a global average ARF of -4.9 ± 0.7 , and $-11.8 \pm 1.9 \text{ W m}^{-2}$ at TOA and surface respectively over land by using a combination of satellite retrievals and model simulations. Li *et al.* [2010] found annual and diurnal mean ARF values of $+0.3 \pm 1.6$, -15.7 ± 8.9 , and $+16.0 \pm 9.2 \text{ W m}^{-2}$ at TOA, surface, and in the atmosphere respectively, throughout China. On a regional scale, our results indicate that aerosol particles in Beijing have small cooling at TOA and moderate warming in the atmosphere under haze events.

combination of SBDART simulations together with ground-based observations. We first calculate the instantaneous ARF in 30 min intervals utilizing the aforementioned approach. To compute the 24 h averaged ARF, we postulate that aerosol concentration remains relatively invariant during the entire day and interpolate AOD and optical properties measurements across periods of cloud present and missing data (including nighttime) to create a continuous time series.

Figure 11 shows the 24 h averaged ARF values at TOA and surface for the three sites. And the ARF in the atmosphere are obtained from ARF at TOA minus those at surface. As shown in Figure 11, ARF values at the three urban sites in Beijing are similar, which is easy to understand. For instance, the daily mean ARF values are slightly negative or neutral at TOA (-30.6 to -4.1 W m^{-2}) but are strongly negative at the surface (-57.0 to -9.9 W m^{-2}) during January of 2013 in Beijing-CAMS site. Accordingly, the ARF values in the atmosphere are moderately positive and range from $+4.5$ to $+26.4 \text{ W m}^{-2}$. Wang *et al.* [2009b] reported the ARF values at the surface, TOA, and in the atmosphere are -76 W m^{-2} , -21 W m^{-2} , and $+55 \text{ W m}^{-2}$, respectively, under a haze day (26 October of 2004) in Beijing. These values are clearly greater than our results (-57.0 , -30.6 , and $+26.4 \text{ W m}^{-2}$) but are still comparable. The overall mean ARF values at the surface are -26.2 ± 12.8 , -26.5 ± 12.7 , and $-26.8 \pm 14.7 \text{ W m}^{-2}$ for the CAMS, IAP and RADI sites, respectively, which are about 2.4 times of the global average $-11.0 \pm 2 \text{ W m}^{-2}$ [Kim and Ramanathan, 2008]. The total mean ARF at TOA are -13.2 ± 7.6 , -12.8 ± 7.5 ,

Figure 12 illustrates the correlative relationship between daily mean ARF and AOD₅₀₀ at the surface and TOA during the whole period. The slopes of best linear fitting are -11.02 , -11.23 , and -11.27 at the surface for the three sites, respectively. The data points are considerably close for all cases, which suggests that aerosol composition remains relatively constant over the Beijing region during January of 2013. The cause of small numbers of scattered points may be partly due to large variations of daily mean SSA and ASY values [Lee *et al.*, 2007]. And the slopes of linear fitting are -4.14 , -3.57 , and -2.56 at TOA for the three sites, respectively.

As discussed above, the ARF values at the surface in Beijing are about 2 times than that at TOA, which suggests that approximately half of the incident solar radiation energy is absorbed by the Earth atmosphere and will eventually heat the atmosphere. We define the heating rate as the rate of atmospheric temperature changes ($\frac{\partial T}{\partial t}$) in a certain layer owing to aerosol-absorbed solar radiation, which can be expressed as

$$\frac{\partial T}{\partial t} = -\frac{1}{\rho C_p} \frac{\Delta F}{\Delta Z} = \frac{g}{C_p} \frac{\Delta F}{\Delta P} \quad (1)$$

where ρ is the density of air and C_p is the specific heat capacity of the air at constant pressure, $\frac{\Delta F}{\Delta Z}$ is the radiative flux divergence, g is the acceleration of gravity, ΔF is the aerosol-absorbed solar energy, and ΔP is the atmospheric pressure difference between the surface and the height of aerosol layer. In this study, we assume that the height of haze layer is 3.2 km (~ 700 hPa) restricted within the planetary boundary layer, which is proved to be reasonable by Li *et al.* [2013b]. ΔF is calculated as the differences in atmospheric absorbed solar radiation with and without aerosols, namely, the ARF in the atmosphere. The daily average heating rate in the haze particle layer (0–3.2 km) vary from 0.12 to 0.68, 0.15 to 0.61, and 0.16 to 0.81 K/day, respectively, for the three sites, corresponding overall mean values of 0.336, 0.356, and 0.433 K/day in Beijing. Such a large diabatic heating might exert profound impact on the atmospheric thermodynamic and dynamical structures and cloud microphysical properties together with the monsoon circulation [Ackerman *et al.*, 2000; Li *et al.*, 2007, 2010; Huang *et al.*, 2006b, 2010], which should be further studied.

5. Summary and Conclusions

In this article, we investigated aerosol optical, microphysical characteristics, and shortwave direct radiative forcing under heavy haze episodes in Beijing during January of 2013. The main data sets are based on three urban sites (CAMS, IAP, and RAD) deployed with Cimel Sun photometers, and two sampling sites observed the concentrations of particulate matters. The principal conclusions of this paper can be summarized as follows.

About 50% of total number days of daily mean PM_{2.5} and PM₁₀ concentrations are larger than 100 $\mu\text{g}/\text{m}^3$, with the maxima of 462 and 433 $\mu\text{g}/\text{m}^3$, respectively, during the severe haze polluted period. The daily averages of SDA fine-mode fraction on 28 January are 0.965, 0.933, and 0.973, respectively, which indicates that small particles are dominant. The overall mean AOD₅₀₀ are 0.71 ± 0.63 , 0.72 ± 0.64 , and 0.51 ± 0.47 for the three sites, corresponding with α values of 1.21 ± 0.21 , 1.19 ± 0.21 , and 1.13 ± 0.26 , respectively. The fine-mode fraction (FMF) significantly increases with Ångström exponent (440–870 nm). The volume size distribution and median radius of fine-mode particles generally increase as AOD₄₄₀ increase. The volume median effective radius of fine-mode particles increases from 0.15 μm at low AOD value (AOD₄₄₀ ~ 0.3) to a radius of 0.25–0.30 μm at high AOD value (AOD₄₄₀ ≥ 1.0) under heavy haze episodes.

The daily mean SSA, imaginary part of refractive index, and ASY displays pronounced spectral behaviors. The overall averages of SSA₄₄₀ and SSA₆₇₅ are 0.892 and 0.905, respectively, while corresponding RI₄₄₀ and RI₆₇₅ are 0.016 and 0.011 under haze cases. This indicates that although haze particles can strongly scatter sunlight, the mean absorption of aerosol in Beijing is very strong during January of 2013. For the Beijing-CAMS site, the overall mean of ARF at the surface, TOA, and in the atmosphere are -26.2 ± 12.8 , -13.2 ± 7.6 , and $+13.0 \pm 6.5$, respectively, which are about 2.4 times of the global average. This incident solar radiation energy absorbed by the Earth atmosphere would go into heating the atmosphere. The daily averaged heating rate in the haze particle layer (0–3.2 km) varies from 0.12 to 0.81 K/day in Beijing, which can exert a profound impact on the atmospheric thermodynamic and dynamical structures and cloud microphysical properties along with the monsoon circulation.

In this study, we only examined the aerosol optical, microphysical, and radiative characteristics under several heavy haze episodes in Beijing. In order to advance our understanding of aerosol-cloud-climate interaction, further efforts should be dedicated to survey more haze cases under different regions over China.

Acknowledgments

SACOL was sponsored by Lanzhou University through 985 Program. This work was jointly supported by the National Basic Research Program of China (2012CB955302 and 2013CB955802), and National Science Foundation of China under grant 41305025 and 41175134. The Fundamental Research Funds for the Central Universities lzujbky-2013-207 and lzujbky-2013-ct05, and the Developmental Program of Changjiang Scholarship and Research Team (IRT1018). We thank the GSFC/NASA AERONET group for processing the AERONET data (<http://aeronet.gsfc.nasa.gov>). The authors would like to express special thanks to the principal investigators at Beijing-CAMS site (Huizheng Che, Chinese Academy of Meteorological Sciences, China Meteorological Administration), Beijing site (Hongbin Chen, Institute of Atmospheric Physics, Chinese Academy of Sciences), and Beijing_RADI site (Zhengqiang Li, Institute of Remote Sensing and Digital Earth of Chinese Academy of Sciences) together with their staff for establishing and maintaining the instruments. We are grateful to the Chinese Environmental Protection Bureau and the U.S. Embassy to provide the daily mean data of PM_{2.5} and PM₁₀ concentrations in Beijing. We appreciate the MODIS and TOMS teams for supplying the satellite data. We would also like to thank all anonymous reviewers for their constructive and insightful comments.

References

- Ackerman, A. S., O. B. Toon, D. E. Stevens, A. J. Heymsfield, V. Ramanathan, and E. J. Welton (2000), Reduction of tropical cloudiness by soot, *Science*, *288*, 1042–1047, doi:10.1126/science.288.5468.1042.
- Beijing Statistical Yearbook (2013), *Beijing Municipal Bureau of Statistics NBS Survey Office in Beijing*, China Statistics Press, Beijing.
- Bergin, M. H., et al. (2001), Aerosol radiative, physical, and chemical properties in Beijing during June 1999, *J. Geophys. Res.*, *106*(D16), 17,969–17,980, doi:10.1029/2001JD900073.
- Bi, J., et al. (2013), Field measurement of clear-sky solar irradiance in Badain Jaran Desert of Northwestern China, *J. Quant. Spectrosc. Radiat. Transfer*, *122*, 194–207, doi:10.1016/j.jqsrt.2012.07.025.
- Bond, T. C., and R. W. Bergstrom (2006), Light absorption by carbonaceous particles: An investigative review, *Aerosol Sci. Tech.*, *40*, 27–67, doi:10.1080/02786820500421521.
- Brook, R. D., et al. (2010), Particulate matter air pollution and cardiovascular disease: An update to the scientific statement from the American Heart Association, *Circulation*, *121*, 2331–2378, doi:10.1161/CIR.0b013e3181d8bec1.
- Chan, C. K., and X. Yao (2008), Air pollution in mega cities in China, *Atmos. Environ.*, *42*, 1–42, doi:10.1016/j.atmosenv.2007.09.003.
- Charlson, R. J., S. E. Schwartz, J. H. Hales, R. D. Cess, J. A. Coakley Jr., J. E. Hansen, and D. J. Hofmann (1992), Climate forcing by anthropogenic aerosols, *Science*, *255*, 423–430, doi:10.1126/science.255.5043.423.
- Che, H., et al. (2009), Instrument calibration and aerosol optical depth validation of the China Aerosol Remote Sensing Network, *J. Geophys. Res.*, *114*, D03206, doi:10.1029/2008JD011030.
- China Statistical Yearbook (2013), *National Bureau of Statistics of China*, China Statistics Press, Beijing.
- Dan, M., G. Zhuang, X. Li, H. Tao, and Y. Zhuang (2004), The characteristics of carbonaceous species and their sources in PM_{2.5} in Beijing, *Atmos. Environ.*, *38*, 3443–3452.
- Dubovik, O., and M. D. King (2000), A flexible inversion algorithm for retrieval of aerosol optical properties from Sun and sky radiance measurements, *J. Geophys. Res.*, *105*, 20,673–20,696, doi:10.1029/2000JD900282.
- Dubovik, O., et al. (2000), Accuracy assessments of aerosol optical properties retrieved from Aerosol Robotic Network (AERONET) Sun and sky radiance measurements, *J. Geophys. Res.*, *105*, 9791–9806, doi:10.1029/2000JD900040.
- Dubovik, O., B. N. Holben, T. F. Eck, A. Smirnov, Y. J. Kaufman, M. D. King, D. Tanré, and I. Slutsker (2002), Variability of absorption and optical properties of key aerosol types observed in worldwide locations, *J. Atmos. Sci.*, *59*, 590–608.
- Dubovik, O., et al. (2006), Application of spheroidal models to account for aerosol particle nonsphericity in remote sensing of desert dust, *J. Geophys. Res.*, *111*, D11208, doi:10.1029/2005JD006619.
- Eck, T. F., B. N. Holben, J. S. Reid, O. Dubovik, A. Smirnov, N. T. O'Neill, I. Slutsker, and S. Kinne (1999), Wavelength dependence of the optical depth of biomass burning, urban and desert dust aerosols, *J. Geophys. Res.*, *104*, 31,333–31,350, doi:10.1029/1999JD900923.
- Eck, T. F., B. N. Holben, D. E. Ward, O. Dubovik, J. S. Reid, A. Smirnov, M. M. Mukelabai, N. C. Hsu, N. T. O'Neill, and I. Slutsker (2001), Characterization of the optical properties of biomass burning aerosols in Zambia during the 1997 ZIBBEE field campaign, *J. Geophys. Res.*, *106*, 3425–3448, doi:10.1029/2000JD900555.
- Eck, T. F., et al. (2005), Columnar aerosol optical properties at AERONET sites in central eastern Asia and aerosol transport to the tropical mid-Pacific, *J. Geophys. Res.*, *110*, D06202, doi:10.1029/2004JD005274.
- Ge, J., J. Su, T. P. Ackerman, Q. Fu, J. Huang, and J. Shi (2010), Dust aerosol optical properties retrieval and radiative forcing over northwestern China during the 2008 China-U.S. joint field experiment, *J. Geophys. Res.*, *115*, D00K12, doi:10.1029/2009JD013263.
- Halthore, R. N., et al. (2005), Intercomparison of shortwave radiative transfer codes and measurements, *J. Geophys. Res.*, *110*, D11206, doi:10.1029/2004JD005293.
- Hao, J., L. Wang, L. Li, J. N. Hu, and X. C. Yu (2005), Air pollutants contribution and control strategies of energy-use related sources in Beijing, *Sci. China, Ser. D Earth Sci.*, *48*(Suppl. II), 138–146.
- He, K., F. Yang, Y. Ma, Q. Zhang, X. H. Yao, C. K. Chan, S. H. Cadle, T. Chan, and P. A. Mulawa (2001), The characteristics of PM_{2.5} in Beijing, China, *Atmos. Environ.*, *35*, 4959–4970.
- He, K., H. Huo, and Q. Zhang (2002), Urban air pollution in China: Current status, characteristics, and progress, *Annu. Rev. Energy Environ.*, *27*, 397–431, doi:10.1146/annurev.energy.27.122001.083421.
- Holben, B. N., et al. (1998), AERONET—A federated instrument network and data archive for aerosol characterization, *Remote Sens. Environ.*, *66*, 1–16.
- Huang, J., B. Lin, P. Minnis, T. Wang, X. Wang, Y. Hu, Y. Yi, and J. K. Ayers (2006a), Satellite-based assessment of possible dust aerosols semi-direct effect on cloud water path over East Asia, *Geophys. Res. Lett.*, *33*, L19802, doi:10.1029/2006GL026561.
- Huang, J., P. Minnis, B. Lin, T. Wang, Y. Yi, Y. Hu, S. Sun-Mack, and K. Ayers (2006b), Possible influences of Asian dust aerosols on cloud properties and radiative forcing observed from MODIS and CERES, *Geophys. Res. Lett.*, *33*, L06824, doi:10.1029/2005GL024724.
- Huang, J., Y. Wang, T. Wang, and Y. Yi (2006c), Dusty cloud radiative forcing derived from satellite data for middle latitude region of East Asia, *Prog. Nat. Sci.*, *10*, 1084–1089.
- Huang, J., P. Minnis, B. Chen, Z. Huang, Z. Liu, Q. Zhao, Y. Yi, and J. K. Ayers (2008), Long-range transport and vertical structure of Asian dust from CALIPSO and surface measurements during PACDEX, *J. Geophys. Res.*, *113*, D23212, doi:10.1029/2008JD010620.
- Huang, J., P. Minnis, H. Yan, Y. Yi, B. Chen, L. Zhang, and J. K. Ayers (2010), Dust aerosol effect on semi-arid climate over Northwest China detected from A-Train satellite measurements, *Atmos. Chem. Phys.*, *10*, 6863–6872, doi:10.5194/acp-10-6863-2010.
- Intergovernmental Panel on Climate Change (2013), *Climate Change 2013: The Physical Science Basis. Contribution of Working Group I to the Fifth Assessment Report of the Intergovernmental Panel on Climate Change*, edited by T. F. Stocker, pp. 1535, Cambridge Univ. Press, Cambridge, U. K., and New York.
- Kaufman, Y. J., I. Koren, L. A. Remer, D. Rosenfeld, and Y. Rudich (2005), The effect of smoke, dust, and pollution aerosol on shallow cloud development over the Atlantic Ocean, *Proc. Natl. Acad. Sci. U.S.A.*, *102*(32), 11,207–11,212, doi:10.1073/pnas.0505191102.
- Kim, D., and V. Ramanathan (2008), Solar radiation budget and radiative forcing due to aerosols and clouds, *J. Geophys. Res.*, *113*, D02203, doi:10.1029/2007JD008434.
- Kotchenruther, R. A., P. V. Hobbs, and D. A. Hegg (1999), Humidification factors for atmospheric aerosols off the mid-Atlantic coast of the United States, *J. Geophys. Res.*, *104*, 2239–2251, doi:10.1029/98JD01751.

- Lee, K. H., Z. Li, M. S. Wong, J. Xin, Y. Wang, W.-M. Hao, and F. Zhao (2007), Aerosol single scattering albedo estimated across China from a combination of ground and satellite measurements, *J. Geophys. Res.*, *112*, D22S15, doi:10.1029/2007JD009077.
- Li, Z., et al. (2007), Aerosol optical properties and their radiative effects in northern China, *J. Geophys. Res.*, *112*, D22S01, doi:10.1029/2006JD007382.
- Li, Z., K.-H. Lee, Y. Wang, J. Xin, and W.-M. Hao (2010), First observation-based estimates of cloud-free aerosol radiative forcing across China, *J. Geophys. Res.*, *115*, D00K18, doi:10.1029/2009JD013306.
- Li, Z., et al. (2013a), Aerosol physical and chemical properties retrieved from ground-based remote sensing measurements during heavy haze days in Beijing winter, *Atmos. Chem. Phys.*, *13*, 10,171–10,183, doi:10.5194/acp-13-10171-2013.
- Li, Z., et al. (2013b), Joint use of active and passive remote sensing for monitoring of severe haze pollution in Beijing 2013 [in Chinese], *J. Remote Sens.*, *17*, 919–928, doi:10.11834/jrs.20133066.
- Li, Z. Q., L. Blarel, T. Podvin, P. Goloub, J. P. Buis, and J. P. Morel (2008), Transferring the calibration of direct solar irradiance to diffuse-sky radiance measurements for CIMEL Sun-sky radiometers, *Appl. Optics*, *47*, 1368–1377, doi:10.1364/Ao.47.001368.
- Molina, M. J., and L. T. Molina (2004), Megacities and atmospheric pollution, *J. Air Waste Manage. Assoc.*, *54*(6), 644–680, doi:10.1080/10473289.2004.10470936.
- Moody, E. G., M. D. King, S. Platnick, C. B. Schaaf, and F. Gao (2005), Spatially complete global spectral surface albedos: Value-added datasets derived from Terra MODIS land products, *IEEE Trans. Geosci. Remote Sens.*, *43*, 144–158, doi:10.1109/TGRS.2004.838359.
- O'Neill, N. T., O. Dubovik, and T. F. Eck (2001), A modified Ångström coefficient for the characterization of sub-micron aerosols, *App. Opt.*, *40*(15), 2368–2374.
- O'Neill, N. T., T. F. Eck, A. Smirnov, B. N. Holben, and S. Thulasiraman (2003), Spectral discrimination of coarse and fine mode optical depth, *J. Geophys. Res.*, *108*, 4559–4573, doi:10.1029/2002JD002975.
- Ramanathan, V., P. J. Crutzen, J. T. Kiehl, and D. Rosenfeld (2001), Aerosols, climate, and the hydrological cycle, *Science*, *294*, 2119–2124, doi:10.1126/science.1064034.
- Reid, J. S., and P. V. Hobbs (1998), Physical and optical properties of young smoke from individual biomass fires in Brazil, *J. Geophys. Res.*, *103*, 32,013–32,030, doi:10.1029/98JD00159.
- Ricchiazzi, P., S. Yang, C. Gautier, and D. Sowle (1998), SBDART: A research and teaching software tool for plane-parallel radiative transfer in the Earth's atmosphere, *Bull. Am. Meteorol. Soc.*, *79*, 2101–2114.
- Schuster, G. L., B. Lin, and O. Dubovik (2009), Remote sensing of aerosol water uptake, *Geophys. Res. Lett.*, *36*, L03814, doi:10.1029/2008GL036576.
- Smirnov, A., B. N. Holben, T. F. Eck, O. Dubovik, and I. Slutsker (2000), Cloud screening and quality control algorithms for the AERONET database, *Remote Sens. Environ.*, *73*, 337–349.
- Sun, Y. L., G. S. Zhuang, A. H. Tang, Y. Wang, and Z. S. An (2006), Chemical characteristics of PM_{2.5} and PM₁₀ in haze-fog episodes in Beijing, *Environ. Sci. Technol.*, *40*, 3148–3155, doi:10.1021/Es051533g.
- Sun, Y. L., et al. (2013), Aerosol composition, sources and processes during wintertime in Beijing, China, *Atmos. Chem. Phys.*, *13*, 4577–4592, doi:10.5194/acp-13-4577-2013.
- U. S. Environmental Protection Agency (EPA) (1990), *Compilation of Air Pollutant Emission Factors*, Stationary point and area sources, vol. 1, U. S. Environmental Protection Agency, Office of Air and Radiation, Office of Air Quality Planning and Standards, Research Triangle Park, N. C.
- U. S. Environmental Protection Agency (EPA) (1991), Technical assistance document for sampling and analysis of ozone precursors, *Rep. EPA 600/8-91-215*, U. S. Environmental Protection Agency, Atmospheric Research and Exposure Assessment Laboratory, Research Triangle Park, N. C.
- Wang, P., W. H. Knap, P. Kuipers Munneke, and P. Stammes (2009a), Clear-sky shortwave radiative closure for the Cabauw Baseline Surface Radiation Network site, Netherlands, *J. Geophys. Res.*, *114*, D14206, doi:10.1029/2009JD011978.
- Wang, Y., et al. (2009b), Aerosol radiative forcing under clear, hazy, foggy, and dusty weather conditions over Beijing, China, *Geophys. Res. Lett.*, *36*, L06804, doi:10.1029/2009GL037181.
- Waston, J. G. (2002), Visibility: Science and regulation, *J. Air Waste Manage. Assoc.*, *52*(6), 628–713, doi:10.1080/10473289.2002.10470813.
- World Health Organization (2005), *Air Quality Guidelines*, Global Update, E87950.
- Xia, X. A., H. B. Chen, P. C. Wang, W. X. Zhang, P. Goloub, B. Chatenet, T. F. Eck, and B. N. Holben (2006), Variation of column-integrated aerosol properties in a Chinese urban region, *J. Geophys. Res.*, *111*, D05204, doi:10.1029/2005JD006203.
- Yu, H., et al. (2006), A review of measurement-based assessments of the aerosol direct radiative effect and forcing, *Atmos. Chem. Phys.*, *6*, 613–666, doi:10.5194/acp-6-613-2006.
- Zhang, R., et al. (2013), Chemical characterization and source apportionment of PM_{2.5} in Beijing: Seasonal perspective, *Atmos. Chem. Phys.*, *13*, 7053–7074, doi:10.5194/acp-13-7053-2013.
- Zheng, M., L. G. Salmon, J. J. Schauer, L. Zeng, C. S. Kiang, Y. Zhang, and G. R. Cass (2005), Seasonal trend in PM_{2.5} source contributions in Beijing, China, *Atmos. Environ.*, *39*, 3967–3976.